Contrib Mineral Petrol (2011) 162:1159–1174
DOI 10.1007/s00410-011-0645-0

ORIGINAL PAPER

Melt evolution in subarc mantle: evidence from heating experiments on spinel-hosted melt inclusions in peridotite xenoliths from the andesitic Avacha volcano (Kamchatka, Russia)

Dmitri A. Ionov · Antoine Bénard · Pavel Y. Plechov

Received: 19 January 2011 / Accepted: 26 April 2011 / Published online: 22 May 2011

Abstract Glass-bearing inclusions hosted by Cr-spinel in harzburgite xenoliths from Avacha are grouped based on homogenization temperatures and daughter minerals into high-T (1,200°C; opx + cpx), intermediate (900–1,100°C; cpx ± amph), and low-T (900°C; amph) and are commonly accompanied by larger "melt pockets". Unlike previous work on unheated inclusions and interstitial glass in xenoliths from Kamchatka, the homogenized glass compositions in this study are not affected by low-pressure melt fractionation during transport and cooling or by interaction with host magma. Primary melt compositions constrained for each inclusion type differ in major and trace element abundances and were formed by different events, but all are silica saturated, Ca-rich, and K-poor, with enrichments in LREE, Sr, Rb, and Ba and negative Nb anomalies. These melts are inferred to have been formed with participation of fluids produced by dehydration of slab materials. The high-T inclusions trapped liquids produced by ancient high-degree, fluid-induced melting in the mantle wedge. The low-T inclusions are related to percolation of low-T melts or hydrous fluids in arc mantle lithosphere. Melt pockets arise from localized heating and fluid-assisted melting induced by rising magmas shortly before the entrapment of the xenoliths. The "high-T" melt inclusions in Avacha xenoliths are unique in preserving evidence of ancient, high-T melting events in arc mantle, whereas the published data appear to characterize pre-eruption enrichment events.

Keywords Melt inclusion · Mantle xenolith · Subduction · Island arc · Hydrous melting · Metasomatism

Communicated by J. Hoefs.

Electronic supplementary material The online version of this article (doi:10.1007/s00410-011-0645-0) contains supplementary material, which is available to authorized users.

D. A. Ionov (✉) · A. Bénard
Université J. Monnet, PRES "Université de Lyon" &
UMR6524-CNRS, 42023 Saint Etienne, France
e-mail: dmitri.ionov@univ-st-etienne.fr

P. Y. Plechov
Department of Geology, Moscow State University,
119899 Moscow, Russia

Introduction

Large-scale upward migration of slab-related fluids and melts takes place in the mantle wedge above sinking oceanic lithosphere (Stern 2002). These melts and fluids are largely responsible for island arc magmatism, mantle metasomatism and, in a broader context, global recycling of volatiles and fluid-mobile elements (van Keken 2003). Some constraints on slab-derived components involved in melting and metasomatism in the mantle wedge can be obtained from studies of arc volcanic rocks (Nakamura et al. 1985) and relevant experimental data. The pristine slab signatures in magmas erupted on the surface, however, can be "blurred" by a number of factors, like crystallization and contamination in the crust, variable proportions of mantle and slab components during melting, and mixing of different slab fluids in the melting zones.

Melt inclusions in magmatic phenocrysts are protected from many of those effects and have been previously studied to get insights into parental melts of arc magmas including those from Kamchatka (Churikova et al. 2007; Danyushevsky et al. 2002; Kamenetsky et al. 1997, 2002; Portnyagin et al. 2007; Schiano 2003; Schiano et al. 2004; Sobolev and Chaussidon 1996). An even more direct approach is to study glass-bearing inclusions in minerals of

mantle xenoliths from modern arc environments, which trapped and preserved melts generated in, or migrating through the wedge (Eiler et al. 2007; Schiano et al. 1995). A difficulty with this approach is that mantle xenoliths, in particular those containing appropriate melt inclusions, are very rare in arc magmas. Furthermore, because the xenoliths may re-equilibrate after partial melting or metasomatism (Soustelle et al. 2010), homogenization (heating and quenching) experiments are necessary to determine liquidus temperatures (T), primary melt compositions, and crystallization history of the inclusions.

Glass-bearing inclusions in mantle xenoliths from the andesitic Avacha volcano in Kamchatka, Russia were earlier reported by Ishimaru and Arai (2009), but those authors did not homogenize the inclusions and mainly reported and discussed data on evolved, silica-rich interstitial glasses, which formed shortly before or during the transport of the xenoliths to the surface. Here, we report petrographic, major and trace element data on a large number of spinel-hosted melt inclusions from harzburgite xenoliths from Avacha including results of homogenization experiments. This paper provides first data on composition of homogenized melt inclusions hosted by residual, Cr-rich spinel from refractory subarc peridotites.

The melt inclusion data are used here to shed more light on melting and metasomatism in subduction zone mantle. We identify two major inclusion types based on their daughter minerals and homogenization temperatures, both are silicic, hydrous, and likely linked to slab sources. The high-T, Mg-rich inclusions (which to the best of our knowledge have not been previously reported from arc mantle xenoliths) appear to have trapped liquids related to melting events in the mantle wedge that produced the refractory harzburgitic residues; the low-T inclusions trapped melts related to recent arc magmatism and metasomatism in the lithospheric mantle.

Geological context and samples

The Avacha strato-volcano is situated in the southern part of the Kamchatka peninsula (53°15′N, 158°51′E) and is part of

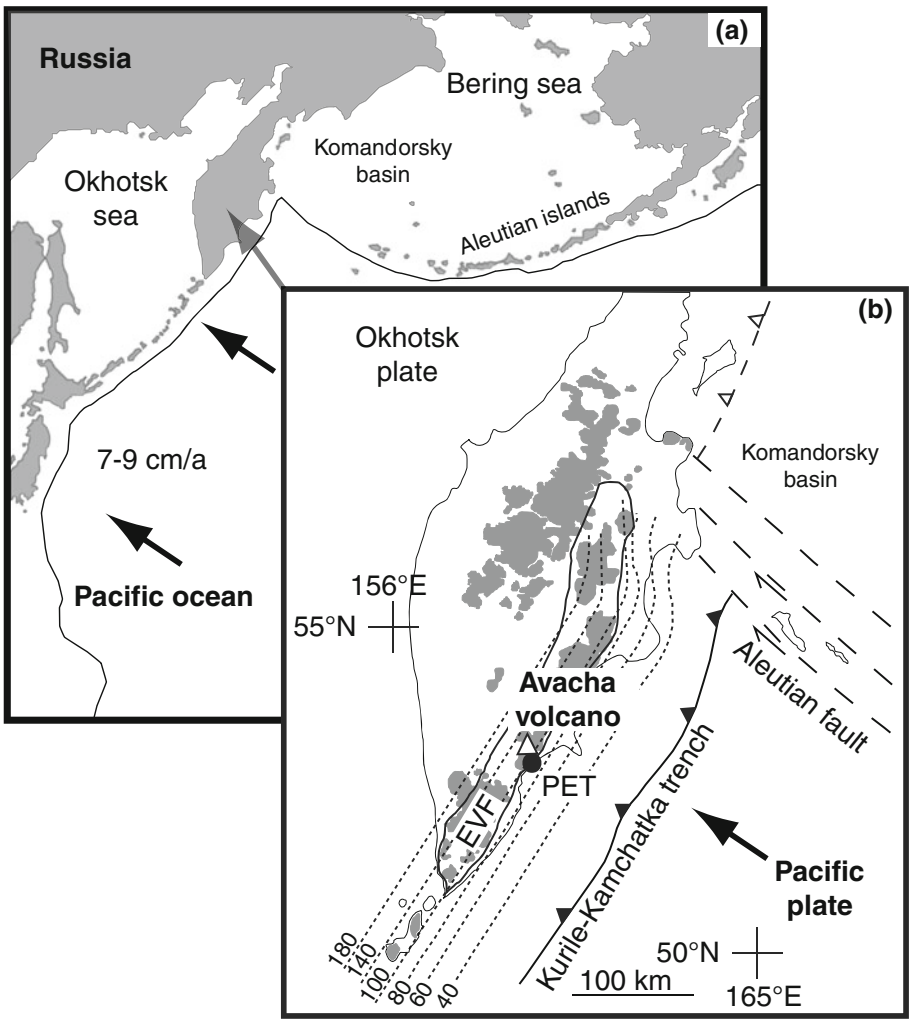

Fig. 1 Location maps for the Avacha volcano. Continuous line in **a** shows position of subduction trenches in western Pacific; *dotted lines* with numbers in **b** show the depth to the *top* of the slab in km; *gray areas* in **b** outline distribution of quaternary volcanic rocks. *EVF* Eastern Volcanic Front, *PET*, the city of Petropavlovsk-Kamchatsky. Modified after (Portnyagin et al. 2007)

its Eastern Volcanic Front (Fig. 1) (Konstantinovskaya 2001). Avacha is one of Kamchatka's most active volcanoes. Its Holocene eruptions produced ashfalls and pyroclastic flows mainly of basaltic and low-K andesite compositions (Braitseva et al. 1998) as well as rare high-Mg olivine basalts and picrite-like "avachites" from flank eruptions (Portnyagin et al. 2005). Seismic data indicate a crustal thickness of ~37 km beneath Avacha (Levin et al. 2002); low P-wave velocities beneath the Moho were interpreted as indicative of the presence of melt (Gorbatov et al. 1999; Manea et al. 2005). The ~80 Ma Pacific plate is subducted beneath the southern Kamchatka arc at a rate of 7–9 cm/a dipping at 55°. Depth of the slab is ~120 km, slab thickness is ~70 km (Gorbatov et al. 1999).

The xenoliths in this study were collected in recent volcanic ash and lapilli deposits. Samples Av14 and Av17 are from a suite of 17 spinel harzburgites reported by Ionov (2010) including petrography, major and trace element composition of bulk rocks and minerals. Other work on the same suite addressed mineral orientation, water contents, and seismic properties (Soustelle and Tommasi 2010), Li, Fe, Mg isotopes (Ionov and Seitz 2008; Pogge von Strandmann et al. 2011; Weyer and Ionov 2007), noble gas compositions (Hopp and Ionov 2011), and sulfide morphology and distribution (Bénard et al. 2011). Xenoliths AP-7, AP-15, and Av33 are similar to those reported by Ionov (2010) in terms of microstructures, modal and major element compositions. The samples were selected for this study based on petrographic inspection, which revealed spinel grains with abundant, large glass-bearing inclusions. Such grains are absent or rare in other Avacha xenoliths in our collection. Spinel grains ranging in size from 0.25 to 1 mm were handpicked from crushed to sieved rocks.

Experiments

Heating and quenching experiments were performed at the Magmatic Petrology laboratory of the Moscow State University (MSU), Russia. The furnace is mounted inside a firebrick. Its heater represents an alundum cylinder 20 mm in diameter and 50 mm long with 40 winds of 0.5 mm platinum wire. A fused quartz sample stage is placed in the middle of the furnace. The work space (thermo-camera) has a diameter of 18 mm, with a Pt-$PtRh_{10}$ thermocouple inserted 0.5 mm below the stage. Spinel grains are placed onto a rectangular platinum sample cell, and each grain is covered with a graphite cap. This platinum cell is inserted into the furnace, which is heated to a desired temperature (T) in advance. The temperature is controlled by the voltage of the MasTech HY-3020E DC power supply. When a sample is placed into the camera, the T usually drops by 5–10 K and recovers in ≤2 min. Samples are quenched by extracting the platinum cell from the furnace (in ≤2 s). The sample is estimated to cool by 400–600 K in the first second. The thermocouples are calibrated with melting T's of pure gold, bismuth, copper, silver, and cadmium. Typical errors on experimental T's reported in this study are ≤0.5%. Horizontal T gradient inside the furnace is ≤3 K for the full working diameter at gold meting point. Heating and quenching experiments were performed separately for spinel with grain size of 0.25–0.5 mm and >0.5 mm. Heating steps were 100°C from 500 to 800°C, 20°C from 800 to 900°C, and 100°C from 900 to 1400°C. Experiment duration was 20 min at <900°C and 6 min at >900°C.

Analytical methods

Back-scattered electron (BSE) and secondary electron (SE) images were obtained using a scanning electron microscope (SEM) at the MSU; phases were identified with energy-dispersive spectroscopy (EDS) on a JEOL JSM-6480LV with an X-ray INCA-Energy-350 Micro-analyzer. Major element analyses were carried out by wavelength-dispersive (WD) electron probe micro-analysis (EPMA) on a CAMECA SX100 instrument at the Laboratoire Magmas et Volcans (LMV, Clermont-Ferrand, France) with accelerating voltage of 15 kV and sample current of 15 nA for minerals and 8, 4, or 2 nA for glasses; defocused electron beam (20, 10 and 5 μm) was used to limit alkali loss in the glass. Counting times were 5–10 s for background and 10–20 s for peaks. Matrix effects were corrected using Phi (r) z Peak Sight© software from CAMECA™. Typical standard deviations (1σ) are 0.1–0.3 wt% for Si, Ca, Na, and Al and 0.03–0.1 wt% for Fe, Cr, K, Ti, Mg, and Mn.

Trace elements were measured by laser ablation–inductively coupled plasma mass-spectrometry (LA-ICPMS) at the LMV on an Agilent 7500 coupled with an UV (193 nm) Excimer Resonetics M-50E laser system in helium flux. Ablation was made at 1–5 Hz and ~12 J cm^{-2} and beam size of 11, 15 and 20 μm. Calibration was made with the NIST 610 glass and Ca as internal standard. NIST 612 and BCR-2 g were measured for quality control, with relative standard deviation (1σ) of 1–4% at ppm abundances (Online Resource 2).

Melt inclusions and pockets: morphology, behavior on heating, major element composition

Melt inclusions (MI) in spinel are <100 μm in size; they have regular (round or isometric) shapes and smooth concave walls (Figs. 2, 4, 5a–c). Melt pockets (MP) in spinel have size up to 300 μm and irregular shapes (Figs. 2c–d, 3c, 5d–f); some are elongated and appear to follow healed cracks (Fig. 2a, b). We subdivide the melt inclusions based

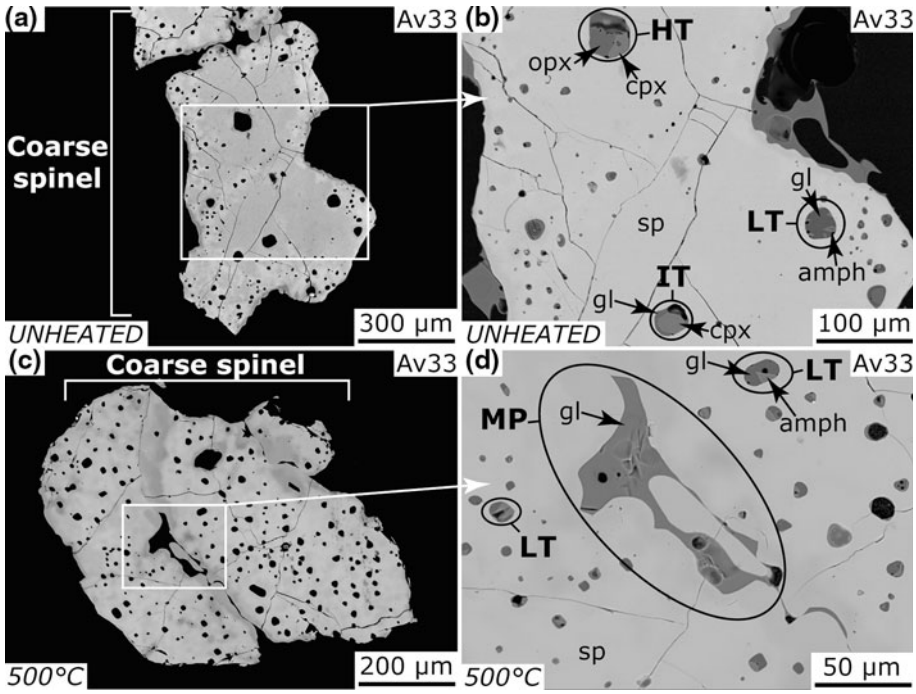

Fig. 2 Back-scattered electron (*BSE*) images of spinel from Avacha xenoliths containing melt inclusions and melt pockets (*MP*). *HT* high temperature inclusion, *LT* low temperature inclusion, *IT* intermediate temperature inclusion, *amph* amphibole, *gl* glass, *sp* spinel; *opx* orthopyroxene, *cpx* clinopyroxene. Each plate has sample number in the *upper-right corner* and a *scale bar* in the *lower-right corner*. See text for discussion

on assemblages of their daughter minerals [orthopyroxene (opx), clinopyroxene (cpx), amphibole (amph)] before heating and homogenization *T*'s and into 3 groups: high temperature (HT) with opx + cpx (Figs. 2d, 4a), intermediate temperature (IT) with cpx ± amph (Fig. 5c), and low temperature (LT) with amph alone (Figs. 2b, d, 5a). The HT inclusions are rare and normally occur in cores of large spl grains (Fig. 2c, d). The LT inclusions occur in inclusion-rich outer parts of large grains (or in inclusion-rich small grains), which look lighter in BSE images. Melt pockets are associated with healed cracks and glass-filled channels. The IT inclusions mainly occur near the boundaries of domains containing the HT and the LT inclusions in complex spinel grains (Fig. 2c, d) and near MP margins (Fig. 5e).

In general, spinels in this study (Online Resource 1) tend to yield higher Cr# $[Cr/(Cr + Al)_{at}]$ (0.61–0.74 vs. 0.54–0.66), lower Mg# $[Mg/(Mg + Fe)_{at}]$ (0.48–0.58 vs. 0.56–0.64), and higher TiO_2 (0–0.4% vs. ≤0.06%) than inclusion-free spinel in the peridotite suite reported by Ionov (2010) (Fig. 3a, b). Spinel next to MI and MP may differ in Cr, Al, Mg, Fe, and Ti abundances from "normal" spinel several tens of micrometers away (Online Resource 1; Fig. 3d, e) apparently due to interaction with trapped melts.

High-temperature (HT) melt inclusions

Unheated HT inclusions we studied are 10–100 μm in size and have round or curved polygonal shapes (Fig. 4a). Glass is subordinate to daughter minerals and may contain bubbles (on the left in Fig. 4a). Predominant daughter phases are subhedral opx and cpx (Fig. 4a). Amphibole is rare (small anhedral grains); it appears to be related to healed cracks (Fig. 4b) and may be secondary. A small (8 μm) melt inclusion with a gas bubble and a submicron daughter spinel crystal are seen in daughter opx in Fig. 4a.

On heating to 900°C, the opx and cpx partially dissolve and become anhedral, and the glass contains small bubbles and may be heterogeneous in the vicinity of the resorbed phases (Fig. 4b). When heated to 1,200°C, large HT inclusions leak but small ones (≤20 μm) usually remain intact (Fig. 4c); all inclusions are decrepitated at 1,300°C (Fig. 5f). The HT inclusions that are intact at 1,200°C consist of homogeneous glass without daughter phases or bubbles. We infer that the entrapment temperature of the HT inclusions is close to 1,200°C. Because the experiments were performed at 1 Pa, homogenization *T*'s at mantle pressures may be higher.

Glasses in unheated HT inclusions have very low totals (87–89 wt%; Table 1). When re-calculated to 100 wt% (volatile free), they yield extremely high SiO_2 (75–77 wt%), which exceed the highest silica contents (72 wt%) reported earlier for glasses in Avacha xenoliths (Ishimaru and Arai 2009) and in intra-plate mantle xenoliths (Ionov et al. 1994; Kaeser et al. 2007; Kluegel 2001 and references therein). Glasses homogenized at 1,200°C have high totals, much lower SiO_2 (56–58 wt%), and higher MgO (10.5–12 wt%), 8.5–9.5 wt% FeO, 12–14 wt% Al_2O_3, 4.0–5.2 wt% CaO, 2–3 wt% Na_2O, and ≤0.2 wt% K_2O (Table 1, Fig. 6b–f). The presence of excess or "captive" cpx or opx (minerals trapped together with melt, often at high mineral/melt ratios) in some of the inclusions before heating may contribute to these variations, in particular for Ca, Mg, and

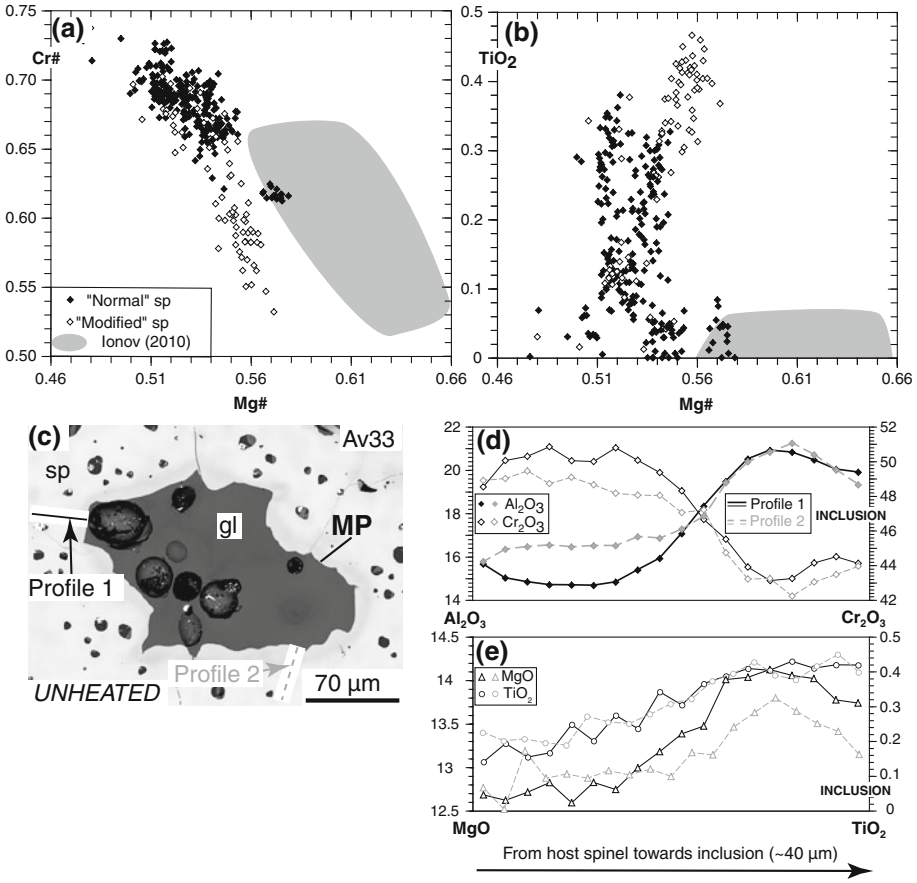

Fig. 3 **a–b** Co-variation plots for Mg# [$Mg/(Mg + Fe)_{at}$], Cr# [$Cr/(Cr + Al)_{at}$] and TiO_2 (wt%) in spinel from this study analyzed far from inclusions ("normal" sp) and close to inclusions and MP ("modified" sp). Gray field outlines spinel compositions (cores of coarse, normally inclusion-free grains) in 17 harzburgite xenoliths from Avacha after Ionov (2010). **c** An BSE image of melt pockets with positions of two EPMA profiles. **d–e** Concentrations (wt%) of Al_2O_3, Cr_2O_3 (**d**), MgO and TiO_2 (**e**) determined by EPMA in two profiles of spinel adjacent to melt pocket shown in **c**

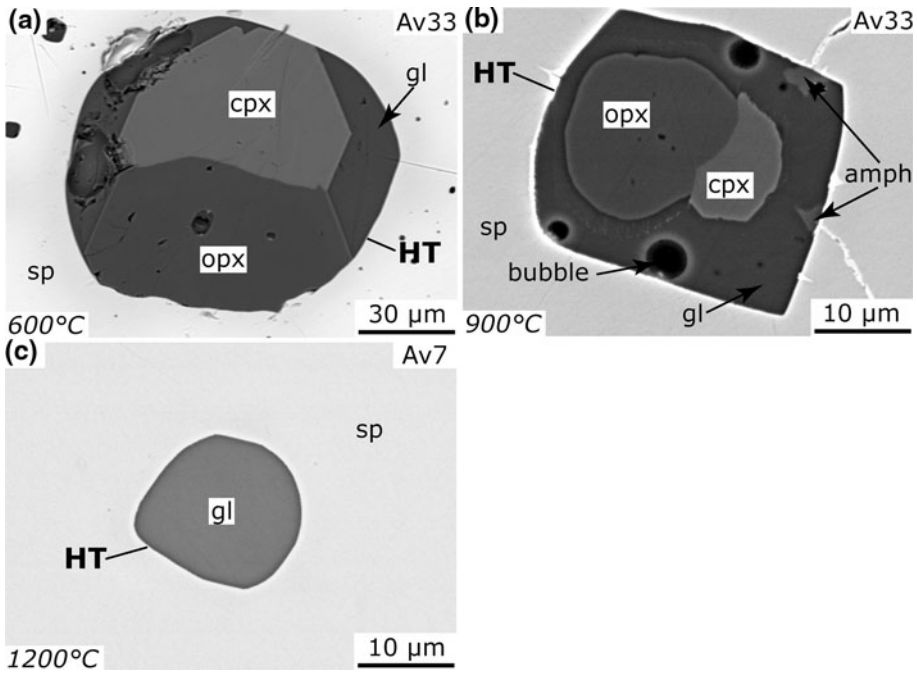

Fig. 4 BSE images of HT inclusions. **a** An opx + cpx + gl inclusion heated to 600°C; the glass (on the *left*) contains vesicles, the opx has a prismatic melt inclusion with a bubble and daughter sp. **b** Resorbed, anhedral opx and cpx in an inclusion heated to 900°C. **c** A small, fully homogenized inclusion at 1,200°C. Each plate has sample number in *upper-right corner* and a *scale bar* in *lower-right corner*

Fe. Importantly, the MgO contents in HT inclusions are higher than in the majority of reported volcanic rocks from Avacha (andesites, basaltic andesites and basalts) except for rare olivine basalts (Fig. 6b; Portnyagin et al. 2005).

Mg# of opx and cpx (0.907–0.922) from unheated HT inclusions (Table 1; Online Resource 1 and 3) are similar to, or slightly lower than, those reported by Ionov (2010) for opx and cpx from Avacha harzburgites. Amphiboles in

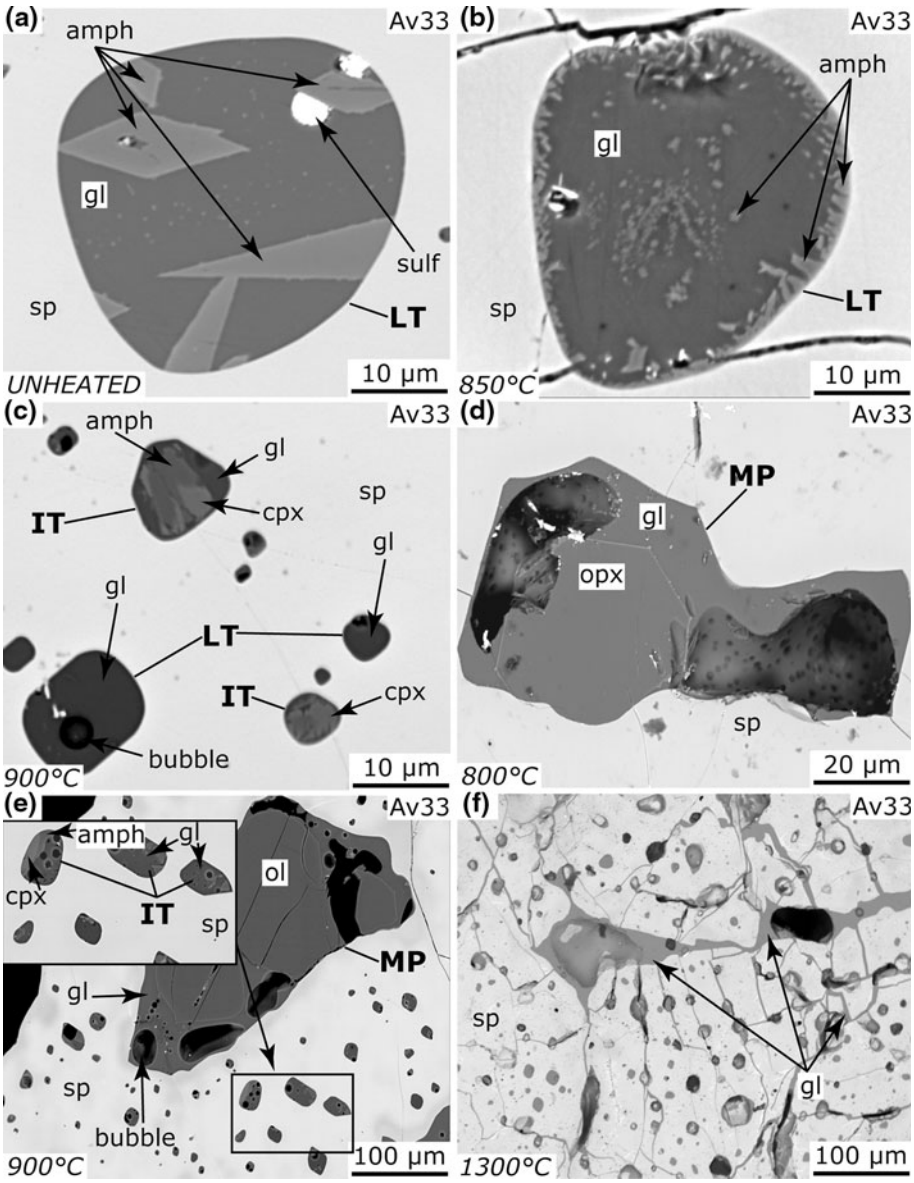

Fig. 5 BSE images of LT and IT inclusions and melt pockets. Abbreviations are the same as in Fig. 2. **a** Euhedral amph and sulfide globules in an unheated LT inclusion. **b** Small, anhedral amph grains in an LT inclusion at 850°C. **c** Homogenized LT inclusions and cpx ± amph-bearing IT inclusions at 900°C. **d** A melt pocket with euhedral opx and vesicles in glass at 800°C. **e** An olivine-bearing melt pocket and nearby IT inclusions containing cpx + amph (900°C). **f** Decrepitated inclusions and melt pockets at 1,300°C. Each plate has sample number in *upper-right corner* and a *scale bar* in *lower-right corner*

HT inclusions have high Mg# (0.915–0.935), low Al_2O_3 (6.6–10 wt%), TiO_2 (0–0.3 wt%), and alkalis (0.1–1.3 wt% Na_2O, 0–0.3 wt% K_2O) (Fig. 7; Table 1 of ES) and are similar to those reported by Ionov (2010). Equilibration T's estimated from pyroxene compositions (Brey and Köhler 1990) range from 1,010 to 1,160°C (opx-cpx: 1,010–1,065°C; Ca-opx: 1,000–1,160°C).

Intermediate-temperature (IT) melt inclusions

IT inclusions are smaller (<50 μm) and more common than HT inclusions. Unheated IT inclusions normally contain anhedral to euhedral cpx and amph in roughly equal amounts, less commonly cpx alone (Figs. 2b, 5c), and rare small (<10 μm) bubbles in glass. On heating to 900°C, cpx and amph remain largely intact (Fig. 5c) in some inclusions and seem to disappear in others (Fig. 5e); small bubbles may appear in the glass. No completely homogenized IT inclusions have been identified in this study because they are hard to distinguish from more numerous LT inclusions at 900°C ≤ T ≤ 1,100°C.

Clinopyroxene in IT inclusions is similar in composition to the cpx in HT inclusions (Online Resource 1, 2); amphibole has lower Mg# (0.78–0.85), higher Al_2O_3 (10.5–13 wt%) and Na_2O (1.8–2.6 wt%), and similar TiO_2 and K_2O (Fig. 7; Online Resource 1). Glasses from unheated to heated (900°C) IT inclusions have EPMA totals of 95–100 wt%. Analyses re-calculated to 100 wt% yield moderate SiO_2 (61.5–66 wt%) and high SO_2 (mainly ~0.3 wt%).

Table 1 Average electron microprobe analyses and normative compositions (wt%) of glass in inclusions

Sa.No°	Av17	Av33	AP7	Av33	Av33	Av33	Av33	Av33	Av33	Av33	Av33
Inclusion type	HT	HT	HT	IT	LT	LT	LT	LT	MP	MP	MP
No. analyses	3	10	14	14	11	5	10	12	15	14	8
Heating T (°C)	Unheated	900°	1,200°	900°	Unheated	500°	900°	1,100°	Unheated	900°	1,100°
SiO_2	67.2	63.3	56.7	63.1	57.5	60.0	58.1	55.9	60.5	60.3	61.7
TiO_2	0.05	0.10	0.03	0.12	0.06	0.04	0.17	0.34	0.43	0.49	0.65
Al_2O_3	12.6	19.4	13.2	19.3	17.3	18.0	19.0	20.9	18.5	19.0	19.6
Cr_2O_3	0.85	0.74	1.17	0.86	0.57	1.05	0.97	1.01	0.55	0.51	1.13
FeO	0.81	1.83	9.17	1.66	1.19	0.72	1.26	1.64	3.09	2.88	2.59
MnO	0.05	0.06	0.14	0.04	0.05	0.05	0.03	0.02	0.07	0.11	0.04
MgO	1.40	1.03	10.92	1.29	0.29	0.34	0.45	0.61	3.26	2.90	0.75
CaO	4.27	6.77	4.56	6.78	6.57	5.16	7.14	6.29	7.40	8.17	6.64
Na_2O	0.51	3.06	2.51	3.88	3.22	3.56	3.75	4.35	4.53	4.13	4.86
K_2O	0.49	0.52	0.10	0.63	0.49	0.60	0.47	0.94	0.75	0.66	1.16
NiO	n.d.	0.01	0.03	n.d.	0.03	n.d.	0.02	0.03	n.d	0.02	0.07
SO_2	0.08	0.26	0.10	0.36	0.68	0.29	1.00	0.55	0.14	0.06	0.09
Total	88.2	97.1	98.7	98.2	87.9	91.9	91.9	92.6	99.4	99.2	99.3
Mg#	0.75	0.50	0.68	0.58	0.30	0.46	0.39	0.40	0.65	0.64	0.34
Normative modal compositions (wt%)											
Quartz	58	28	10	23	28	29	24	15	11	12	13
Plagioclase	28	59	44	65	63	60	66	70	68	68	72
Orthoclase	3	3	1	4	3	4	3	6	4	4	7
Corundum	5	2	2	1	1	4	2	3	–	–	–
Diopside	–	–	–	–	–	–	–	–	6	7	2
Hypersthene	6	5	41	6	3	2	3	4	9	8	4

HT high temperature, *IT* intermediate temperature, *LT* low temperature, *MP* melt pocket, *n.d.* not detected,; Mg# = $Mg/(Mg + Fe)_{at}$

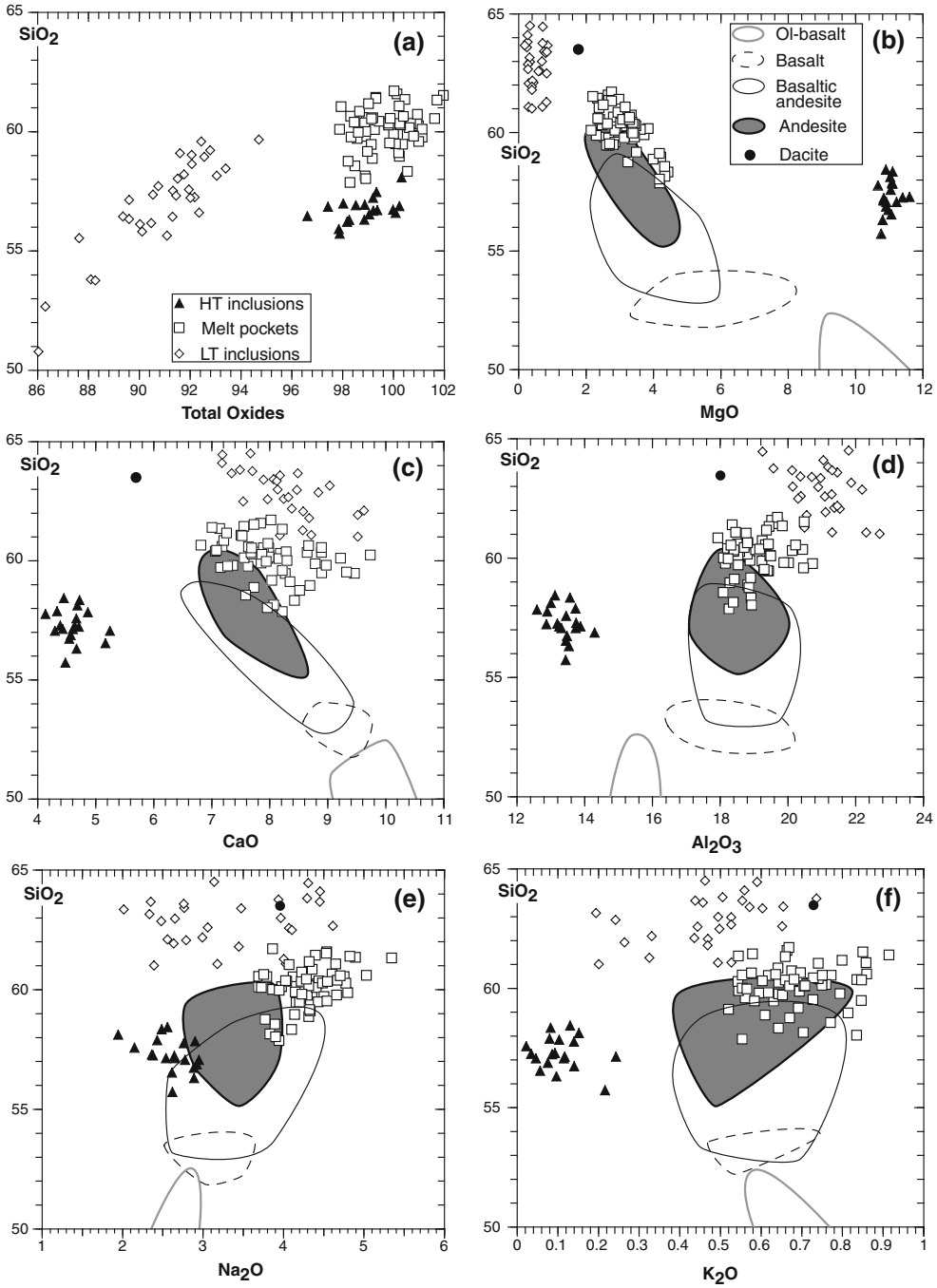

Fig. 6 Co-variation plots of EPMA (wt%) of homogenized inclusions (HT, *filled triangles*; LT, *empty rhombs*) and melt pockets (*empty squares*). No data for IT inclusions are plotted because no fully homogenized IT inclusions have been identified with certainty. Also shown are fields for volcanic rocks from Avacha after (Portnyagin et al. 2005). **a** SiO_2 vs. EPMA totals. **b–f** SiO_2 vs. MgO, CaO, Al_2O_3, Na_2O and K_2O concentrations normalized to 100% (volatile free)

Low-temperature (LT) melt inclusions

LT inclusions are by far the most common. They are <50 μm in size, some are elongated (Fig. 2b–d). Unheated inclusions contain prismatic to acicular amph, abundant glass (≥50%), rare sulfide globules, and unidentified submicron phases and bubbles (Fig. 5a). Amphiboles in the LT and IT inclusions are similar in composition (Fig. 7). On heating, relict amph may persist at 850°C (Fig. 5b) but it dissolves entirely at 900°C (Fig. 5c).

Glasses in homogenized (at 900–1,100°C) LT inclusions yield variable but generally low totals (85–95 wt%). Analyses re-calculated to 100% show the highest SiO_2 (61–64.5 wt%) and Al_2O_3 (20–22.7 wt%) and lowest FeO (≤2 wt%) and MgO (≤1 wt%) in this study as well as high SO_2 (mainly ~0.5 wt%). EPMA mapping of homogenized inclusions shows S-enriched domains 2–3 μm across and strong Na zoning, with 3.5–4.2 wt% Na_2O at inclusion rims and 2–3 wt% Na_2O in the core; other elements appear to be distributed homogeneously.

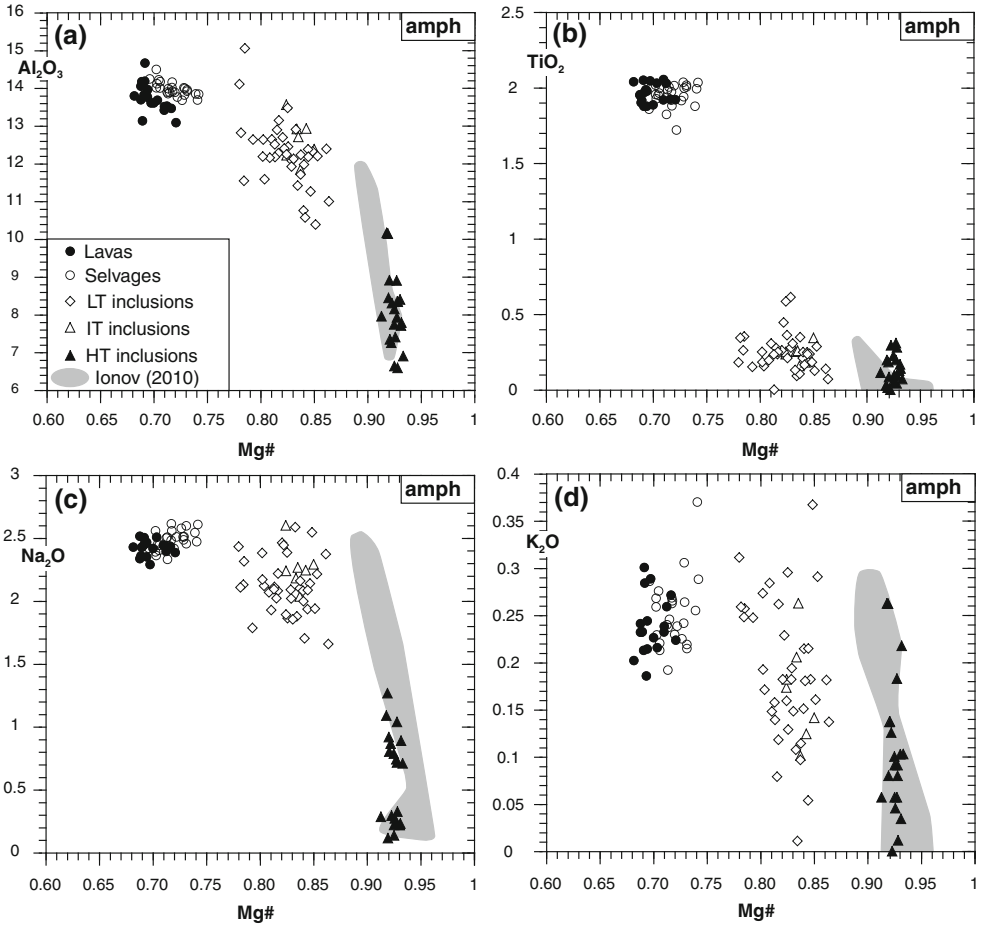

Fig. 7 Co-variation plots of EMPA data on amphibole from host lava (*filled circles*), selvages (*empty circles*), LT (*rhombs*), IT (*empty triangles*), and HT (*filled triangles*) inclusions. Gray field outlines amph compositions in Avacha harzburgite xenoliths after Ionov (2010)

Melt pockets

Melt pockets usually consist of glass with large, round (Fig. 3c), or irregularly shaped vesicles, but may also contain euhedral opx (≤50 μm; Fig. 5d) or subhedral olivine (Fig. 5e). Major element distribution in unheated MP glass is homogeneous based on EPMA mapping, with totals not far from 100 wt% (Fig. 6a). The MP glass is intermediate in composition between those for HT and LT inclusions for SiO_2 (59–61.5 wt%), Al_2O_3 (18–21 wt%), MgO, and FeO (2–4 wt%) and has the highest Na_2O (3.7–5.3 wt%) and K_2O (0.5–0.9 wt%); SO_2 is <0.2 wt%. The MP and LT glasses have high CaO (7–9.5 wt%) similar to that in basaltic andesite from Avacha (Fig. 6c). Olivine Mg# in the MP (0.90–0.91) as well as Ni and Mn contents are similar to or slightly lower than for olivine from the host peridotites (Mg# 0.905–0.92; Online Resource 1 and 3). Mg# of opx in the MP is much lower (∼0.81, Table 1) than for opx in the host peridotites (0.907–0.924; Online Resource 3).

Heating experiments at ≥1,100°C yield equivocal results because the liquids produced escape through cracks and mix with those from decrepitated inclusions to form networks of melt channels (Fig. 5f). Glass in MP heated to >1,200°C is low in silica, likely due to reaction with host spinel.

Trace elements

Representative trace element analyses of glasses from homogenized LT inclusions and MP and of cpx from unheated HT inclusions are given in Online Resource 2 and illustrated in Fig. 8. No trace element data have been obtained on homogenized HT and IT inclusions because the LA-ICPMS detection limits are too low when using narrow laser beams necessary to analyze these small (<20 μm) targets.

Clinopyroxenes from unheated HT inclusions are very low in REE (REE_N ∼ 0.1–1 where "N" shows abundances normalized to primitive mantle values after Hofmann (1988)), with LREE-depleted patterns and positive Sr anomalies (Fig. 8a).

The MP analyses show little spot-to-spot variation. The shapes of their patterns and LREE/HREE values ($(La/Er)_N$ ∼ 2) are similar to those of two Avacha andesites

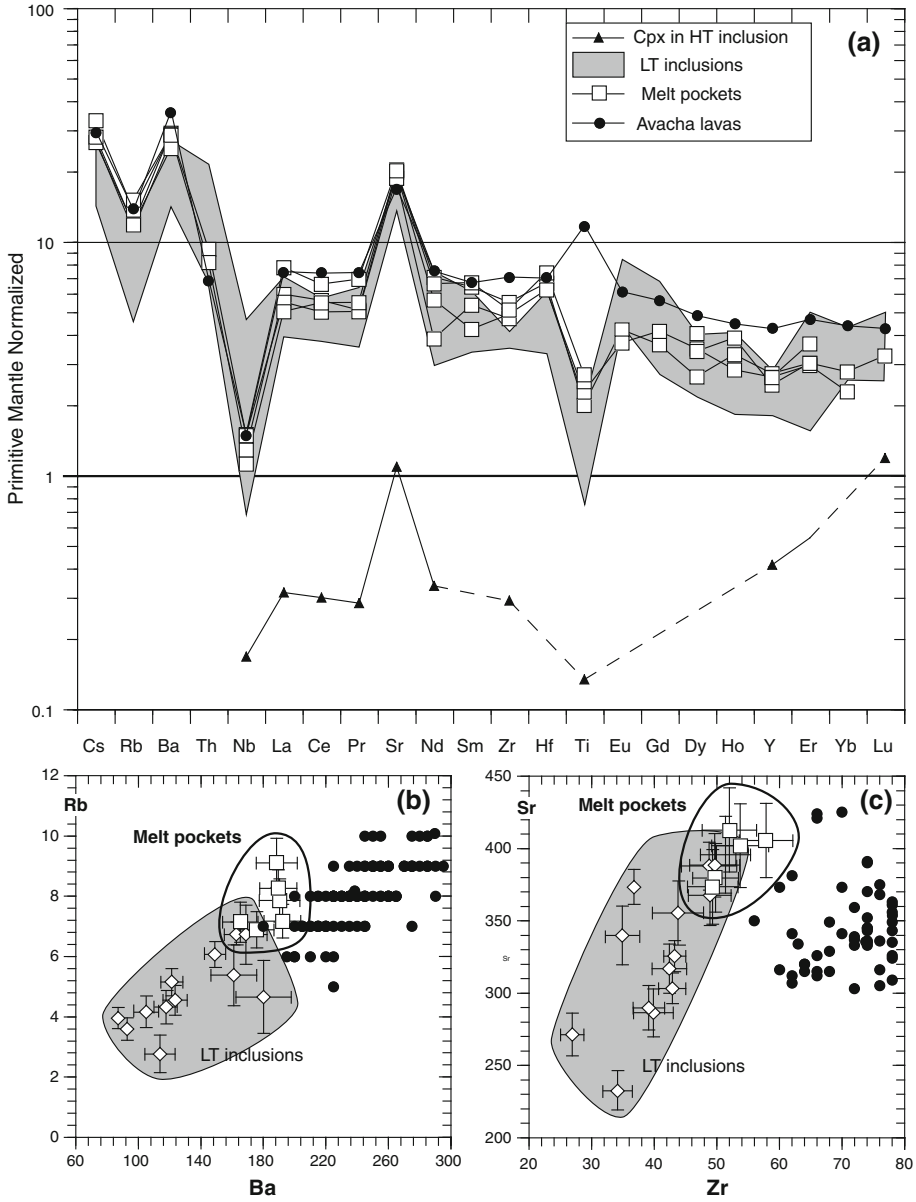

Fig. 8 **a** Primitive mantle-normalized (Hofmann 1988) trace element patterns for melt pockets (*empty squares*), LT inclusions (*gray field*), and a daughter cpx (*filled triangles*) from this study and Holocene lavas (*black dots*, average) after (Ishimaru et al. 2007). **b**, **c** Co-variation plots of element abundances (ppm) for LT inclusions, melt pockets, and host lavas (Castellana 1998; Ishimaru et al. 2007) (*symbols* are same as in Fig. 6). See discussion in text

reported by (Ishimaru et al. 2007) ($(La/Er)_N$ 1.6–1.8; Fig. 8a). The MP glasses, however, have lower Y, Zr, and Ba and tend to have lower REE ($La_N = 5$–7.8, $Er_N = 2.5$–3.7) than the andesites ($La_N \sim 7.5$, $Er_N = 4.1$–4.7). Like the host andesites, the MP glasses are rich in highly incompatible, fluid-mobile elements (Cs, Rb, Ba, with similar $(Rb/Ba)_N = 0.4$–0.5) and have Sr spikes ($(Sr/Nd)_N = 3$–5) and negative Nb anomalies ($(Nb/La)_N = 0.2$–0.3), but show no significant Zr and Hf anomalies (Fig. 8a). By contrast, the MP glasses have strong negative Ti anomalies ($(Ti/Eu)_N = 0.3$–0.6) whereas the host andesites show Ti spikes ($(Ti/Eu)_N = 1.5$–1.9).

Trace element patterns of homogenized LT inclusions are very similar to those of MP but the concentration range is greater for the former (Fig. 8a). Like the MP, the LT inclusions have negative Ti anomalies ($(Ti/Eu)_N = 0.05$–0.4) and lower LREE ($La_N = 4$–7) and $(Zr/Hf)_N$ (0.3–0.8 vs. 0.7–0.8) than the host andesites. Taken together, the LT inclusion and MP data define positive co-variation trends for Cs, Rb, Ba, Sr, and Zr; the MP generally have higher abundances of these highly incompatible elements (Fig. 8b, c). The contents of Y, Ba, and Zr in the LT inclusions and MP are lower than in Holocene volcanic rocks from Avacha (Castellana 1998). The volcanic rocks plot off the MP-LT trends on some of these diagrams (Fig. 8c) further indicating that the parental liquids of the MP and LT inclusions cannot be produced by fractionation of parental magmas of the Holocene volcanic rocks.

Relation to earlier work

Pockets of interstitial silicate glass have been found in many suites of mantle xenoliths worldwide (e.g., Ionov et al. 1994; Neumann and Wulff-Pedersen 1997; Schiano and Bourdon 1999). By contrast, melt inclusions in minerals of peridotite mantle xenoliths are much less common and their preservation may require special conditions. Spinel appears to be an excellent "micro-container" for melt inclusions due to its chemical and physical stability and high elasticity (Kamenetsky et al. 2001; Shimizu et al. 2001). Comparisons with experimental data suggest that the compositions of homogenized melt inclusions in spinel are consistent with P–T equilibration conditions of the host xenoliths and are not significantly affected during the capture and transport of the xenoliths by host magma (Schiano et al. 1998, 2000). Hence, melt inclusions can be used to infer melt compositions and P–T conditions during melting and metasomatism in the mantle (Schiano et al. 1994). By comparison, interstitial glasses in mantle xenoliths are strongly affected by low-pressure crystal fractionation and melt-rock interaction during their transport to the surface and cooling (Schiano and Bourdon 1999), and their compositions may be very different from those of their parental mantle melts.

Post-capture effects on melt inclusion compositions

Glass analyses in this study yield high Cr_2O_3 (0.3–1.0 wt% in unheated inclusions and up to 1.8 wt% in homogenized inclusions) whereas Cr_2O_3 contents estimated for trapped melts based on spinel-melt equilibrium models (e.g., Ariskin and Nikolaev 1996) are much lower (0.03–0.07 wt% at 1,200°C, 0.1 GPa and NNO fO_2 buffer), consistent with data on spinel-bearing natural glasses (Kamenetsky et al. 2001). The Cr_2O_3 measured in the glass may roughly indicate the share of spinel it "assimilated" and thus enable to reconstruct initial melt compositions using analyses of "normal" spinel and assuming its "stoichiometric" assimilation by melt. Typical corrected values for each inclusion type are presented in Online Resource 1. The melt inclusions may have been enriched in Cr_2O_3 by 0.3–1.0 wt% and in FeO by 0.1–0.4 wt% and depleted in Al_2O_3 by ≤0.9 wt%, in MgO by ≤0.2 wt%, and in TiO_2 by ≤0.04 wt%. Apart from Cr, Al, and Fe, these corrections are minor relative to compositional variations in each inclusion type and MP (Fig. 6) and are neglected below.

EPMA profiles across the walls of some unheated melt pockets (Fig. 3c–e) and LT inclusions show important variations of Cr, Al, Mg, and Ti in spinel near the walls apparently due to melt-host interaction after the entrapment. Variable compositional gradients in opposite inclusion walls (Fig. 3c–e) suggest that the melt-host reaction is a complex disequilibrium process and that its effects on glass composition may not be assessed precisely using simple assimilation models. Oxide contents in homogenized inclusions might also be affected by selective (non-stoichiometric) cation exchange with host spinel during heating (e.g., Danyushevsky et al. 2002), in particular for Fe considering its rapid diffusion and an order of magnitude concentration difference (17–23 wt% FeO in sp vs. 0.7–3 wt% in glass), with important effects for Mg#.

Melt entrapment in spinel at different evolution stages of the mantle beneath Avacha

Ionov (2010) and Soustelle et al. (2010) identified several events in the mantle beneath Avacha based on petrologic, trace element, and micro-structural data on peridotite xenoliths. These events can be grouped in three major evolution stages. (1) The earliest event was an extensive fluid-induced melting (28–35%) in the asthenosphere; the melting residues slowly cooled to ≤900°C and were incorporated into the lithosphere. (2) The lithospheric source region of the xenoliths experienced brittle deformation and infiltration of hydrous fluids and melts, which precipitated accessory amph in peridotites (Ionov 2010) and formed coarse pyroxenite veins (Halama et al. 2009). (3) The latest mantle event recorded in the xenolith suite was a combination of localized heating, re-crystallization (Soustelle et al. 2010), and intrusion of thin, quenched magmatic veins (Bénard and Ionov 2010) shortly before the eruption of host magma. Lastly, during the transport to the surface, amph-rich "selvages" precipitated on the surface of the xenoliths (and in some cases thin veins formed along cracks inside) from the host magma.

The finding of distinct groups of MI and MP in this study with different trapping *T*'s and compositions is consistent with the inferences of the earlier work that the lithospheric mantle beneath Avacha underwent a multi-stage evolution and reacted with different melts and fluids at different *T*'s in the past. The melt inclusion data shed more light on relations between the nature of these melts and fluids and the evolution of arc mantle.

(1) The trapping *T* for the HT inclusions (≥1,200°C) estimated in this study falls within the *T* range of mantle hydrous melting from experimental data. Vapor-saturated melting (in the presence of an H_2O-rich supercritical fluid) of a fertile peridotite begins at 940°C at 1.2 GPa (Grove et al. 2006) and may proceed to *T*'s of 1,100–1,345°C (at 1.2–2.0 GPa), with up to 12 wt% H_2O dissolved in the liquid (Gaetani and Grove 1998). Toward the upper limit of

this T range, such melts are in equilibrium with highly refractory harzburgite (olivine + opx ± Cr-spl) residues (Grove et al. 2003), which formed a protolith for the Avacha peridotite suite (Ionov 2010). The homogenization T of the HT inclusions is not particularly high (≥1,200°C), yet their parental liquids may have been equilibrated with harzburgitic (cpx free) residues because melting degrees increase roughly linearly with the abundance of water added to the system (Hirschmann et al. 1999), i.e., cpx may be exhausted in the residue at moderate T's if much water is added. Furthermore, the melt was likely trapped by spinel from interstitial liquid when it began to solidify, i.e., at somewhat lower T's than at the peak of melting. The HT inclusions may have also trapped liquids produced by reaction of high-T hydrous melts with adjacent less refractory mantle rocks. Lower equilibration T's for the HT inclusions from pyroxene thermometry (1,010–1,160°C) may reflect uncertainties of the T estimates (which presume olivine + opx + cpx equilibria) or, alternatively, crystal fractionation due to decreasing T's after the entrapment. Importantly, these values are well above homogenization T's for the LT inclusions. Overall, the HT inclusions appear to have sampled liquids produced by high-degree fluid-induced melting in the asthenosphere or by interaction of such melts with mantle wedge rocks. Low $^{187}Os/^{188}Os$ ratios reported for Avacha harzburgites similar to xenoliths in this study (Widom et al. 2003) indicate that the melting took place long time ago. Water for melting came from slab-derived fluids, which also contributed fluid-mobile trace elements.

(2) The LT melt inclusions may be related to percolation of hydrous fluids or low-T melts in the arc mantle lithosphere. The lowest T estimates for the Avacha xenoliths from opx and ol-spl thermometry (≤900°C; Ionov (2010)) and for the LT inclusions from heating experiments (850–900°C) agree well with each other. Refractory harzburgites cannot melt at such low T's; vapor-saturated melting of fertile peridotites at 1.2 GPa begins at 940°C (Grove et al. 2006). Hence, the LT melt inclusions may have "sampled" products of reaction of migrating supercritical hydrous fluids with host refractory mantle. We speculate that the same slab-derived fluids also produced accessory amph as well as coarse, amph-bearing pyroxenite veins in the Avacha harzburgites (Halama et al. 2009; Hopp and Ionov 2011). The IT inclusions may have formed by mixing of LT-type fluids with existing HT inclusions.

(3) Melt pockets likely formed at a later stage concurrent with localized heating and re-crystallization (Ishimaru and Arai 2009). The texturally non-equilibrated morphology and large size of the MP's suggest an origin due to local, fluid-assisted melting. These phenomena may have been related to heating and fluid circulation related to transport of andesitic melts through the lithospheric mantle shortly before the entrapment of the xenoliths (Ionov 2010) as also inferred for many xenolith suites in alkali basalts (Ionov et al. 1994; Kaeser et al. 2007).

It is essential to distinguish the melt-rock interaction events that took place in the mantle (stages 2–3 above) from the effects of host andesitic magma on mantle xenoliths during their capture and transport to the surface (e.g., Kluegel 2001). The surface of mantle xenoliths from Avacha (if present in xenolith fragments collected in the field) is coated with "selvages" 1–5 mm in thickness made up mainly of euhedral black amphibole rich in Fe and Ti (Mg# < 0.75; 1.7–2.1 wt% TiO_2). Petrographic and EPMA data show the presence of interstitial glasses and Fe–Ti enrichments inside xenoliths several mm from their rims. Some xenoliths also contain sheet-like black amph-rich veins filling cracks linked to the selvages, such veins formed from host magmas (or fluids derived from host magmas) injected into fractures in the xenoliths during their transport. The in situ melting and Fe–Ti enrichments caused by host magmas may be mistaken for mantle metasomatic events when observed in small xenolith fragments. For instance, Ionov (2010) found no interstitial glass in central parts of large and fresh peridotite xenoliths from Avacha whereas Ishimaru and Arai (2009) and Ishimaru et al. (2007) reported common silicate glass in small, re-crystallized xenoliths. Importantly, amph in all inclusion types have much higher Mg# and lower TiO_2 than amph from the selvages and host andesites (Fig. 7). A general advantage of melt inclusion data in this study is that they are not affected by interaction with host magma and other very recent events; we also note that the spinel in this study comes from central parts of large xenoliths that contain no veins and no interstitial silicate glass except for spinel-hosted MP associated with melt inclusions.

The composition and origin of parental melts of HT and LT inclusions and MP

The compositional fields of HT inclusions do not overlap (and usually plot far apart from) those of LT inclusions and MP in Fig. 6. Homogenized HT inclusions, in particular, have lower SiO_2, CaO, Al_2O_3, and alkalis and higher MgO and FeO (EPMA normalized to 100%) than LT inclusions and MP. These important chemical differences are a major argument for a distinct nature of their parental melts

together with much higher homogenization T, the presence of opx among daughter minerals, and consistently high Mg# (≥0.91) in the pyroxenes and amph. The parental melts of the HT inclusions are chemically similar to basaltic andesite liquids produced experimentally by hydrous mantle melting (e.g., Gaetani and Grove 1998; Grove et al. 2003) and may have initially equilibrated with refractory melting residues, like the inferred protoliths of the Avacha harzburgite series (Ionov 2010).

While the LT and MP compositions are largely distinct, they partly overlap on co-variation plots of some major oxides (SiO_2, alkalis) and trace elements (Figs. 6, 8b, c). It is conceivable that these materials be linked to evolution from a common source or a series of related melts. The latter could be produced by dehydration of slab materials and may represent metasomatic agents migrating in the cold (~900°C) mantle lithosphere.

All homogenized glass compositions in this study are silica saturated, with 10 wt% of normative quartz for HT inclusions and 12–25% for LT inclusions and MP (Table 1). Such compositions can be attributed to hydrous partial melting in the mantle wedge fluxed by slab-derived fluids. Slab signatures are also obvious in trace element patterns of the LT inclusions and MP, notably enrichments in LREE, Sr and fluid-mobile Cs, Rb, and Ba as well as a strong negative Nb anomaly (Fig. 8) (e.g., Churikova et al. 2007; Portnyagin et al. 2007). The similarities in the LT and MP patterns (Fig. 8a) and common chemical co-variation trends (Fig. 8b, c) support genetic links between their parental melts inferred from major elements and low homogenization T's. Trace element patterns of the LT and MP mimic those of host andesites from Avacha (Fig. 8a) with an important exception of Zr and Ti, which show minor positive anomalies in the andesites but negative anomalies in the LT and MP. The latter may be an artifact due to the loss of Ti to spinel (Fig. 5e), which together with Fe–Ti oxides can host Ti and Zr in the mantle (Bodinier et al. 1996; Kalfoun et al. 2002). The similarities in trace element patterns, together with common major oxide affinities, like low alkalis and high CaO (Fig. 6), may suggest that parental melts of the LT inclusions and MP originate from the same source as Avacha volcanic rocks.

Published data on homogenized melt inclusions from arc mantle xenoliths are very rare; nearly all are for xenoliths from the Batan Island in the Philippines (Schiano et al. 1995). The major and trace element compositions of melt inclusions and MP from this study differ greatly from those from Batan (Fig. 9). In particular, the Batan inclusions

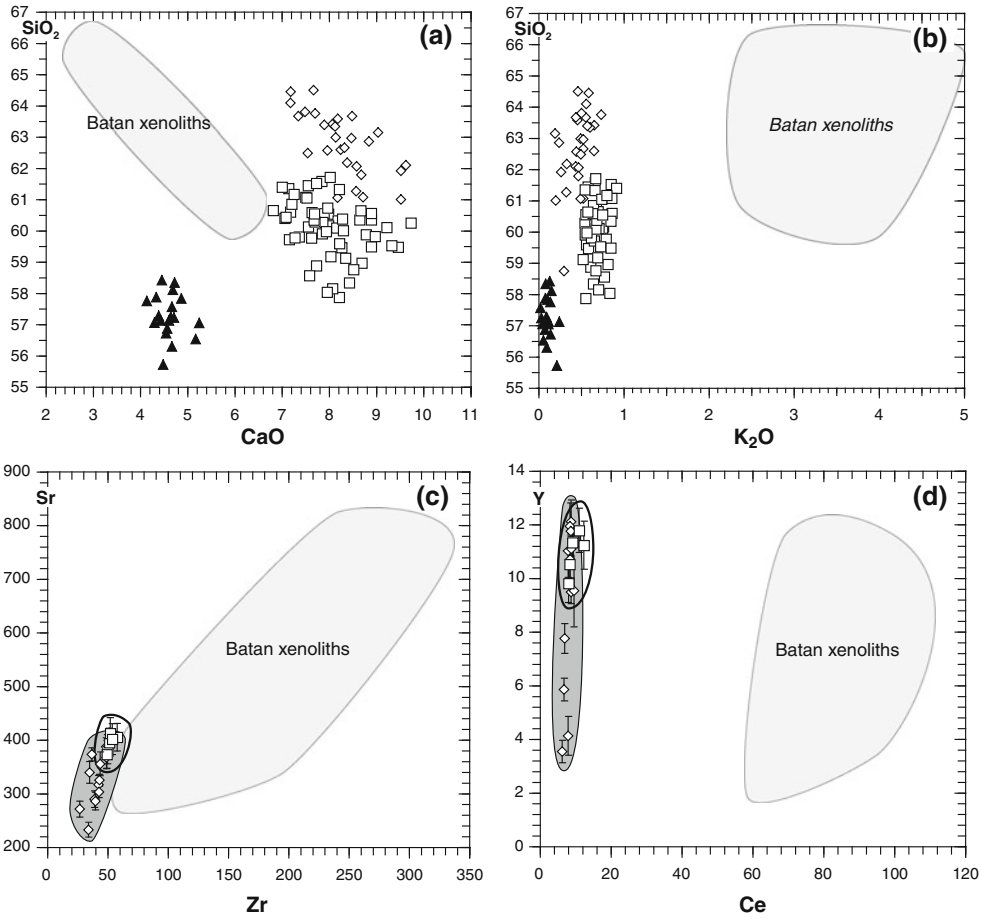

Fig. 9 Element co-variation plots for melt inclusions from this study (*symbols* are same as in Fig. 6) compared with the field for melt inclusions in xenoliths from Batan in the Philippines (Schiano et al. 1995). Major oxides are normalized to 100% totals (volatile free)

have much higher abundances of alkalis and incompatible trace elements (LREE, Zr; Fig. 9c, d). The distinct melt inclusion compositions are consistent with petrographic and chemical differences between the two xenolith suites. Contrary to the peridotites in this study (Ionov 2010), the Batan xenoliths are strongly metasomatized, i.e., they contain veins and accessory mica as well as more abundant amph and have higher whole-rock abundances of alkalis, Ti, and incompatible trace elements (Maury et al. 1992; Vidal et al. 1989). Hence, the Batan xenoliths may have been more affected by late-stage melt/fluid circulation in the mantle. The Avacha xenoliths appear to be unique currently in preserving evidence of much earlier mantle events including partial melting (HT inclusions).

Conclusions

(1) Glass-bearing spinel-hosted inclusions in harzburgite xenoliths from Avacha are grouped, based on homogenization *T*'s and daughter mineral assemblages, into high-*T* (1,200°C; opx + cpx), intermediate (900–1,100°C; cpx ± amph), and low-*T* (900°C; amph) and are accompanied by larger, irregularly shaped "melt pockets" (ol + opx).

(2) By contrast to published data on interstitial glass and unheated inclusions from Avacha xenoliths, the glass compositions obtained in homogenization experiments in this study are not affected by (a) low-pressure melt fractionation during transport and cooling or (b) interaction with host magma, which affected xenolith rims and formed Fe–Ti–rich amphibole veins and coatings.

(3) Primary melt compositions determined for the HT and LT inclusions and MP define distinct fields on major oxide co-variation plots. The HT inclusions appear to have sampled liquids produced by high-degree, fluid-induced melting in the asthenosphere or by interaction of such melts with mantle wedge rocks. The LT inclusions are related to percolation of hydrous fluids or low-*T* melts in the arc mantle lithosphere. Melt pockets formed later, shortly before the entrapment of the xenoliths, due to localized heating and fluid-assisted melting in the deep lithosphere induced by rising magma.

(4) All homogenized inclusions and melt pockets are silica saturated and ultimately stem from slab-derived fluids related to dehydration of slab materials. Slab signatures are also seen in trace element patterns, notably enrichments in LREE, Sr, Cs, Rb, and Ba and strong negative Nb anomalies.

(5) Melt inclusions in the Avacha xenoliths may be unique in preserving evidence of relatively old events in the arc mantle including partial melting (HT inclusions) and metasomatism compared with published data, which may mainly document recent, likely eruption-related events.

Acknowledgments V. D. Scherbakov designed and assembled the heating stage used in this work. Analytical and technical assistance was provided by C. Alboussière and V. O. Yapaskurt. DAI acknowledges a PNP grant from Institut National de Sciences de l'Univers (INSU—CNRS, France) in 2010. We appreciate advice from V. Kamenetsky, constructive reviews by T. Churikova and A. Klügel and editorial handling by J. Hoefs.

References

Ariskin AA, Nikolaev GS (1996) An empirical model for the calculation of spinel-melt equilibria in mafic igneous systems at atmospheric pressure: 1. Chromian spinels. Contrib Miner Petrol 123(3):282–292

Bénard A, Ionov DA (2010) Melt-rock interaction in supra-subduction mantle: evidence from veined peridotites from the Avacha volcano, Kamchatka. Geophys Res Abstr 12:EGU2010–EGU2112

Bénard A, Palle S, Doucet LS, Ionov DA (2011) Three-dimensional imaging of sulfides in silicate rocks at sub-micron resolution with multi-photon microscopy. Microsc Microanal (in press)

Bodinier J-L, Merlet C, Bedini RM, Simien F, Remaidi M, Garrido CJ (1996) Distribution of niobium, tantalum, and other highly incompatible trace elements in the lithospheric mantle: the spinel paradox. Geochim Cosmochim Acta 60(3):545–550

Braitseva OA, Bazanova LI, Melekestsev IV, Sulerzhitskiy LD (1998) Large Holocene eruptions of Avacha volcano, Kamchatka (7250–3700 14C years B.P.). Volcanol Seismol 20(1):1–27

Castellana B (1998) Geology, chemostratigraphy, and petrogenesis of the Avachinskiy volcano, Kamchatka, Russia. PhD thesis, University of California, Los Angeles, 365 p

Churikova T, Wörner G, Mironov N, Kronz A (2007) Volatile (S, Cl and F) and fluid mobile trace element compositions in melt inclusions: implications for variable fluid sources across the Kamchatka arc. Contrib Mineral Petrol 154(2):217–239

Danyushevsky LV, McNeill AW, Sobolev AV (2002) Experimental and petrological studies of melt inclusions in phenocrysts from mantle-derived magmas: an overview of techniques, advantages and complications. Chem Geol 183(1–4):5–24

Eiler JM, Schiano P, Valley JW, Kita NT, Stolper EM (2007) Oxygen-isotope and trace element constraints on the origins of silica-rich melts in the subarc mantle. Geochem Geophys Geosyst 8:Q09012. doi:10.1029/2006GC001503

Gaetani GA, Grove TL (1998) The influence of water on melting of mantle peridotite. Contrib Mineral Petrol 131:323–346

Gorbatov A, Dominguez J, Suarez G, Kostoglodov V, Zhao D, Gordeev E (1999) Tomographic imaging of the P-wave velocity structure beneath the Kamchatka peninsula. Geophys J Int 137(2): 269-279. doi:10.1046/j.1365-246X.1999.t01-1-00801.x

Grove TL, Elkins-Tanton LT, Parman SW, Chatterjee N, Muntener O, Gaetani GA (2003) Fractional crystallization and mantle-melting controls on calc-alkaline differentiation trends. Contrib Mineral Petrol 145(5):515–533

Grove TL, Chatterjee N, Parman SW, Medard E (2006) The influence of H2O on mantle wedge melting. Earth Planet Sci Lett 249(1–2):74–89

Halama R, Savov I, Rudnick R, McDonough W (2009) Insights into Li and Li isotope cycling and sub-arc metasomatism from veined mantle xenoliths, Kamchatka. Contrib Miner Petrol 158(2):197–222

Hirschmann MM, Asimov PD, Ghiorso MS, Stolper EM (1999) Calculation of peridotite partial melting from thermodynamic models of minerals and melts. III. Controls on isobaric melt production and the effect of water on melt production. J Petrol 40:831–851

Hofmann AW (1988) Chemical differentiation of the earth: the relationship between mantle, continental crust, and oceanic crust. Earth Planet Sci Lett 90:297–314

Hopp J, Ionov DA (2011) Tracing partial melting and subduction-related metasomatism in the Kamchatkan mantle wedge using noble gas compositions. Earth Planet Sci Lett 302(1–2):121–131. doi:10.1016/j.epsl.2010.12.001

Ionov DA (2010) Petrology of mantle wedge lithosphere: new data on supra-subduction zone peridotite xenoliths from the andesitic Avacha volcano, Kamchatka. J Petrol 51(1–2):327–361

Ionov DA, Seitz HM (2008) Lithium abundances and isotopic compositions in mantle xenoliths from subduction and intra-plate settings: mantle sources versus eruption histories. Earth Planet Sci Lett 266(3–4):316–331

Ionov DA, Hofmann AW, Shimizu N (1994) Metasomatism-induced melting in mantle xenoliths from Mongolia. J Petrol 35(3):753–785

Ishimaru S, Arai S (2009) Highly silicic glasses in peridotite xenoliths from Avacha volcano, Kamchatka arc; implications for melting and metasomatism within the sub-arc mantle. Lithos 107(1–2):93–106

Ishimaru S, Arai S, Ishida Y, Shirasaka M, Okrugin VM (2007) Melting and multi-stage metasomatism in the mantle wedge beneath a frontal arc inferred from highly depleted peridotite xenoliths from the Avacha volcano, southern Kamchatka. J Petrol 48(2):395–433. doi:10.1093/petrology/egl065

Kaeser B, Kalt A, Pettke T (2007) Crystallization and breakdown of metasomatic phases in graphite-bearing peridotite xenoliths from Marsabit (Kenya). J Petrol 48(9):1725–1760

Kalfoun F, Ionov D, Merlet C (2002) HFSE residence and Nb-Ta ratios in metasomatised, rutile-bearing mantle peridotites. Earth Planet Sci Lett 199(1–2):49–65

Kamenetsky VS, Crawford AJ, Eggins S, Mühe R (1997) Phenocryst and melt inclusion chemistry of near-axis seamounts, Valu Fa Ridge, Lau Basin: insight into mantle wedge melting and the addition of subduction components. Earth Planet Sci Lett 151:205–223

Kamenetsky VS, Crawford AJ, Meffre S (2001) Factors controlling chemistry of magmatic spinel: an empirical study of associated olivine, Cr-spinel and melt inclusions from primitive rocks. J Petrol 42(4):655–671

Kamenetsky VS, Sobolev AV, Eggins SM, Crawford AJ, Arculus RJ (2002) Olivine-enriched melt inclusions in chromites from low-Ca boninites, Cape Vogel, Papua New Guinea: evidence for ultramafic primary magma, refractory mantle source and enriched components. Chem Geol 183(1–4):287–303

Kluegel A (2001) Comment on "Silicic melts produced by reaction between peridotite and infiltrating basaltic melts: ion probe data on glasses and minerals in veined xenoliths from La Palma, Canary Islands" by Wulff-Pedersen et al. Contrib Mineral Petrol 141(4):505–510

Konstantinovskaya EA (2001) Arc-continent collision and subduction reversal in the Cenozoic evolution of the Northwest Pacific: an example from Kamchatka (NE Russia). Tectonophysics 333:75–94

Levin V, Park J, Brandon M, Lees J, Peyton V, Gordeev E, Ozerov A (2002) Crust and upper mantle of Kamchatka from teleseismic receiver functions. Tectonophysics 358(1–4):233–265

Manea VC, Manea M, Kostoglodov V, Sewell G (2005) Thermal models, magma transport and velocity anomaly estimation beneath southern Kamchatka. In: Foulger GR, Natland JH, Presnall DC, Anderson DL (eds) Plates, plumes, and paradigms. Geological Society of America Special Publications Paper 388, Boulder, pp 517–536

Maury RC, Defant MJ, Joron J-L (1992) Metasomatism of the sub-arc mantle inferred from trace elements in Philippine xenoliths. Nature 360:661–663

Nakamura E, Campbell IH, Sun S-S (1985) The influence of subduction processes on the geochemistry of Japanese alkaline basalts. Nature 316:55–58

Neumann E-R, Wulff-Pedersen E (1997) The origin of highly silicic glass in mantle xenoliths from the Canary Islands. J Petrol 38(11):1513–1539

Pogge von Strandmann PAE, Elliott T, Marschall HR, Coath C, Lai Y-J, Jeffcoate A, Ionov DA (2011) Variations of Li and Mg isotope ratios in bulk chondrites and mantle xenoliths. Geochim Cosmochim Acta (in press)

Portnyagin MV, Plechov PY, Matveev SV, Osipenko AB, Mironov NL (2005) Petrology of avachites, high-magnesian basalts of Avachinsky volcano, Kamchatka: I. General characteristics and composition of rocks and minerals. Petrologiya 13(2):99–121

Portnyagin M, Hoernle K, Plechov P, Mironov N, Khubunaya S (2007) Constraints on mantle melting and composition and nature of slab components in volcanic arcs from volatiles (H2O, S, Cl, F) and trace elements in melt inclusions from the Kamchatka Arc. Earth Planet Sci Lett 255(1–2):53–69

Schiano P (2003) Primitive mantle magmas recorded as silicate melt inclusions in igneous minerals. Earth-Sci Rev 63(1–2):121–144

Schiano P, Bourdon B (1999) On the preservation of mantle information in ultramafic nodules: glass inclusions within minerals versus interstitial glasses. Earth Planet Sci Lett 169(1–2):173–188

Schiano P, Clocchiatti R, Shimizu N, Weis D, Mattielli N (1994) Cogenetic silica-rich and carbonate-rich melts trapped in mantle minerals in Kerguelen ultramafic xenoliths: Implications for metasomatism in the oceanic upper mantle. Earth Planet Sci Lett 123:167–178

Schiano P, Clocchiatti R, Shimizu N, Maury RC, Jochum KP, Hofman AW (1995) Hydrous, silica-rich melts in the sub-arc mantle and their relationships with erupted arc lavas. Nature 377:595–600. doi:10.1038/377595a0

Schiano P, Bourdon B, Clocchiatti R, Massare D, Varela ME, Bottinga Y (1998) Low-degree partial melting trends recorded in upper mantle minerals. Earth Planet Sci Lett 160:537–550

Schiano P, Clocchiatti R, Bourdon B, Burton KW, Thellier B (2000) The composition of melt inclusions in minerals at the garnet–spinel transition zone. Earth Planet Sci Lett 174(3–4):375–383

Schiano P, Clocchiatti R, Boivin P, Medard E (2004) The nature of melt inclusions inside minerals in an ultramafic cumulate from Adak volcanic center, Aleutian arc: implications for the origin of high-Al basalts. Chem Geol 203(1–2):169–179

Shimizu K, Komiya T, Hirose K, Shimizu N, Maruyama S (2001) Cr-spinel, an excellent micro-container for retaining primitive melts—implications for a hydrous plume origin for komatiites. Earth Planet Sci Lett 189(3–4):177–188

Sobolev AV, Chaussidon M (1996) H2O concentrations in primary melts from supra-subduction zones and mid-ocean ridges: implications for H2O storage and recycling in the mantle. Earth Planet Sci Lett 137:45–55

Soustelle V, Tommasi A (2010) Seismic properties of the supra-subduction mantle: constraints from peridotite xenoliths from the Avacha volcano, southern Kamchatka. Geophys Res Lett 37(13):L13307

Soustelle V, Tommasi A, Demouchy S, Ionov DA (2010) Deformation and fluid-rock interaction in the supra-subduction mantle:

microstructures and water contents in peridotite xenoliths from the Avacha volcano, Kamchatka. J Petrol 51(1–2):363–394

Stern RJ (2002) Subduction zones. Rev Geophys 40(4):1012. doi: 1010.1029/2001RG000108

van Keken PE (2003) The structure and dynamics of the mantle wedge. Earth Planet Sci Lett 215(3–4):323–338

Vidal P, Dupuy C, Maury R, Richard M (1989) Mantle metasomatism above subduction zones: trace-element and radiogenic isotope characteristics of peridotite xenoliths from Batan Island (Philippines). Geology 17:1115–1118

Weyer S, Ionov DA (2007) Partial melting and melt percolation in the mantle: the message from Fe isotopes. Earth Planet Sci Lett 259(1–2):119–133

Widom E, Kepezhinskas P, Defant MJ (2003) The nature of metasomatism in the sub-arc mantle wedge: evidence from Re-Os isotopes in Kamchatka peridotite xenoliths. Chem Geol 196(1–4):283–306